Facile preparation of self-healing hydrogels based on chitosan and PVA with the incorporation of curcumin-loaded micelles for wound dressings

Peng Ding[1,2,ζ,*], Xiaoyue Ding[1,ζ], Jingyu Li[1], Wei Guo[1], Oseweuba Valentine Okoro[3], Mahta Mirzaei[4,5], Yanfang Sun[6], Guohua Jiang[7,8], Amin Shavandi[3], and Lei Nie[1,2,*]

[1] School of Life Science, Xinyang Normal University, Xinyang464000, China

[2] Tea Plant Biology Key Laboratory of Henan Province, Xinyang Normal University, Xinyang 464000, China

[3] Université libre de Bruxelles (ULB), École polytechnique de Bruxelles - BioMatter unit, Avenue F.D. Roosevelt, 50 - CP 165/61, 1050 Brussels, Belgium

[4] Centre for Food Chemistry and Technology, Ghent University Global Campus, Incheon, South Korea

[5] Department of Food Technology, Safety and Health, Faculty of Bioscience Engineering, Ghent University, Coupure Links 653, geb. A, B-9000 Ghent, Belgium

[6] School of Materials Science and Engineering, Zhejiang Sci-Tech University, Hangzhou 310018, China

[7] International Scientific and Technological Cooperation Base of Intelligent Biomaterials and Functional Fibers, Zhejiang Sci-Tech University, Hangzhou 310018, China

[8] Centre for Food Chemistry and Technology, Ghent University Global Campus, Incheon, South Korea.

[ζ] Co-first authors.

*** Corresponding authors:**

Prof. Lei Nie

nieleifu@yahoo.com; nielei@xynu.edu.cn

Dr. Peng Ding

dingzhiyu120@163.com

Abstract

The increased demand for improved strategies for wound healing has, in recent years, motivated the development of multifunctional hydrogels with favorable bio-compatibility and antibacterial properties. To this regard, the current study presented the design of a novel self-healing composite hydrogel that could perform as wound dressing for the promotion of wound healing. The composite hydrogels were composed of polyvinyl alcohol (PVA), borax and chitosan functionalized with sialic acid (SA-CS) and curcumin loaded Pluronic F127 micelles. The hydrogels were formed through the boronic ester bond formation between PVA, SA-CS and borax under physiological conditions and demonstrated adjustable mechanical properties, gelation kinetics and antibacterial properties. When incubating with NIH3T3 cells, the hydrogels also demonstrated good biocompatibility. These aspects offer a promising foundation for their prospective applications in developing clinical materials for wound healing.

Keywords: Chitosan, hydrogel, boronic ester bond, curcumin, wound healing

1. Introduction

Wounds constitute skin defects that are prevalent in human history and are recognized as increasing the risk of endogenous bacterial infection, which can negatively influence human health [1-11]. These wounds are healed via a complex process involving hemostasis, inflammation, proliferation and remodeling steps that overlapped and incorporated the action of several cell types, such as platelets, endothelial cells etc [12-15]. Meanwhile, wound healing, in some cases, e.g. diabetic wounds, may require more time to be repaired, thus increasing the risk of infections and exacerbating the potential of more serious (i.e. necrosis) and life-threatening difficulties occurring [16-26]. It is, therefore, crucial to synthesize functional wound dressings which promote wound healing while having innate antibacterial properties. To this regard, various biomaterials, such as foams [27, 28], films [29, 30], nanosheets [31], and hydrogels [10, 32-38] have been developed. In this strategy, the hydrogels with the injectable and antibacterial properties were considered as the most promising biomaterial because of their tunable excellent antibacterial and self-healing properties, which will serve to enhance the overall efficiency of wound healing.

Thus, a functional hydrogel could become an excellent tool for preventing wound infection and accelerating wound healing. For addressing this issue, hydrogels derived from natural polysaccharide-based biomaterials have received extraordinary attention. This is due to their inherent desirable biocompatibility, making them a promising candidate for a myriad of applications in the Biomedical industry [39-49]. Chitosan (CS) is a non-toxic, biodegradable and biocompatible amino polysaccharide produced

from the chitin that is present in the exoskeletons (shells) of arthropods and cell walls of fungi [50]. As one of the most abundant natural materials, it has also been widely utilized as a biomaterial because of its biocompatible and antibacterial properties. Notably, its poor solubility in solvents (i.e. polar or non-polar) limits its versartility[51, 52]. Therefore, chitosan is usually chemically modified with different functional groups to enhance its bioactivity through reactions with primary or secondary hydroxyl groups on the chitosan backbone [30, 50, 53, 54]

Curcumin (Cur), known as isopropyl methane, is present in the turmeric herb and is reported to possess favourable biological properties such as anti-inflammatory, hypoglycemic, wound healing properties, etc., making it potentially beneficial to human health [55-57]. Cur is, however, also characterized by poor solubility in water, poor bioavailability, and poor stability in light [57, 58]. Due to these limitations, previous works have incorporated the encapsulation of Cur into a suitable carrier, such as hydrogel, for transporting to the target tissue [59-61].

Herein, inspired by proteoglycan in the extracellular matrix, we fabricated polysaccharide-based composite hydrogels composed of borax, sialylated chitosan, PVA, and curcumin-loaded Pluronic F127 micelles, characterized with inherent self-healing and antibacterial properties (**Scheme 1**). Ingeniously, the dynamic ester bonds between PVA, sialylated chitosan and borax endow these hydrogels with the capacity to fill any irregularly shaped wound. **Scheme 1** also shows that the study will promote improved bioavailability of Cur by undertaking its micellization for enhanced delivery in water-mediated hydrogels. Due to these design improvements, it is anticipated that

the hydrogel may be employed to promote wound healing and therapeutic effects while also limiting the risk of wound infections.

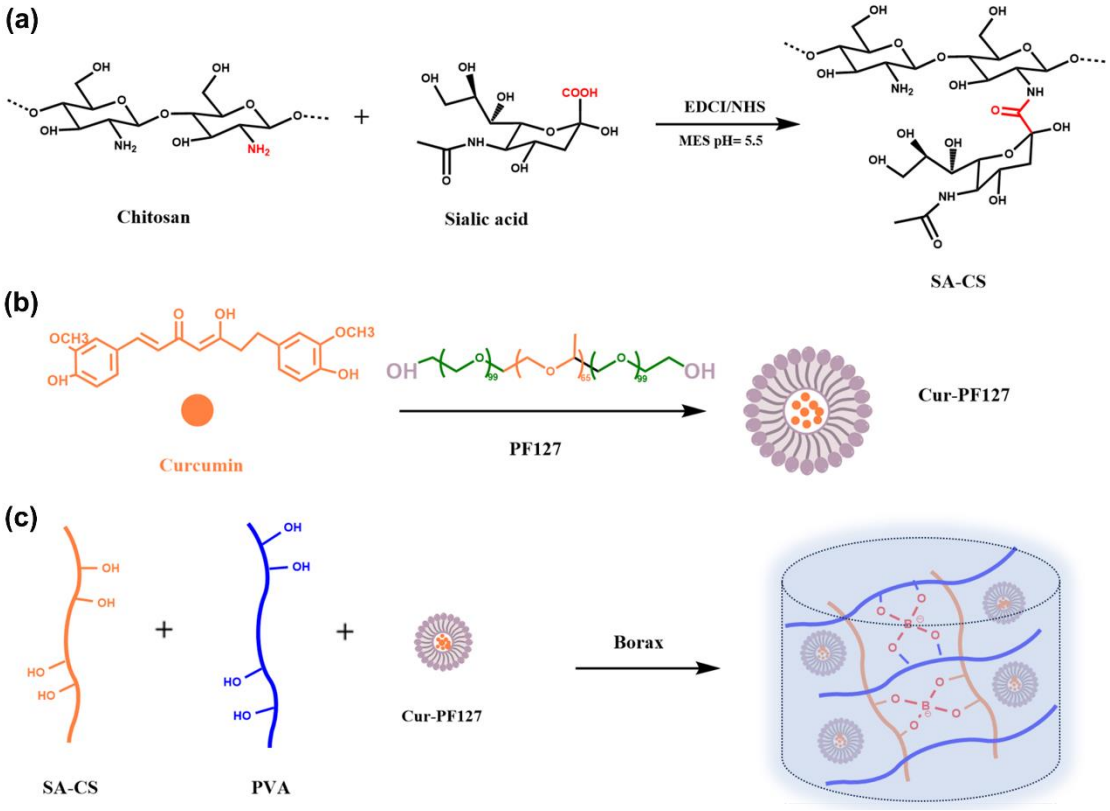

Scheme 1. Scheme showing the synthesis of sialylated chitosan (SA-CS) and curcumin-loaded PF127 micelles (Cur-PF127), and the fabrication of composite hydrogel based on SA-CS, PVA, Cur-PF127, and Borax.

2. Materials and methods

2.1 Materials

In the study, Aladdin industrial corporation (Shanghai, China) was the supplier of morpholinoethanesulfonic acid (MES), chitosan (CS, degree of deacetylation: ca. 95%), N-hydroxysuccinimide (NHS), 1-ethy-3-(3-dimethylaminopropyl carbodiimide) hydrochloride (EDC•HCl) and sialic acid. Sodium tetraborate decahydrate and other

reagents were bought from Sinopharm, China.

2.2 Synthesis of sialic acid-conjugated chitosan (SA-CS)

1.8 g of chitosan was initially dissolved in 220 mL of 1 % acetic acid aqueous solution. After this, 5 M NaOH was introduced to the solution in a dropwise manner to adjust the pH to 6. Sialic acid (1.0 g), NHS (0.45 g) and EDCI (0.74 g) were then dissolved in 0.1M MES buffer (pH = 5.0), and stirred 0.5 h and then added into chitosan solution. The solution was then reacted for 12 h at room temperature under gentle stirring. After 12 h, the obtained solution was dialyzed for 72 h against distilled water while employing a 7000 Da dialysis membrane. After the dialysis, the solution was freeze-dried.

2.3 Preparation of curcumin loaded Pluronic F127 micelles (Cur-PF127)

The one-step solid dispersion method was used in the preparation of Cur-PF127 micelles [59]. Briefly, a certain amount of curcumin and Pluronic 127 polymer at the feed ration of 1:99 were dissolved in dichloromethane with gentle stirring, and then the solution was condensed in a rotary evaporator at 40 ^{o}C. Finally, the co-evaporation was dissolved in H_2O at 40 ^{o}C under continuous stirring to self-assemble into micelles, followed by lyophilization to obtain the yellow Cur-PF127 powder.

2.4 Synthesis of Borax-assisted Cur-PF127/SA-CS/PVA hydrogels

SA-CS polymer and PVA were separately dissolved in phosphate-buffered saline (5 mL, PBS) at a pH of 7.2 at 37 ^{o}C to prepare a mixed solution containing SA-CS (3.5% w/v) and PVA (3.5% w/v). Then, 0.000 g, 0.001g, 0.015g, and 0.025g Cur-PF127 were respectively added to the aforementioned mixed solution to make the

concentration of Cur-PF127 at 0%, 1%, 3%, and 5% (w/v). Subsequently, 900 μL 4 % wt of borax was introduced to the mixture solution and vortexed to obtain a series of composite hydrogels referred to as Gel 1 to Gel 4, respectively.

2.5 Morphology of hydrogels

Gold was employed in coating the hydrogels, after initial freezing in liquid nitrogen and drying for 12 h. The gold-coated samples were then analyzed with a scanning electron microscope (SEM; Hitachi, S-4800).

2.6 Antioxidant activity

The ABTS (7 mM) solution was mixed with (2.5 mM) potassium persulfate for oxidation in the dark for 12–16 h at room temperature to prepare ABTS·+. This ABTS·+ solution was then employed in measuring the antioxidant activity. Then 0.05g of the sample to be tested was added to the ABTS·+ solution (5 mL), and the mixture was oscillated and incubated in the dark at 37 ºC for 30 min. Finally, the absorbance of the reaction solution was measured at 734 nm. The free radical scavenging efficiency was calculated as follows :

$$ABTS\ Scavenging\ (\%) = \frac{[A]_{Blank} - [A]_{Sample}}{[A]_{Blank}} \times 100\% \quad (1)$$

Where $[A]_{Blank}$ denotes the absorption of the blank and $[A]_{Sample}$ denotes the absorption of the sample. Herein, the blank refers to the ABTS solution only, and the sample solution refers to the ABTS + sample solution.

2.7 Rheological evaluations

Rheological measurements of the composite hydrogels were undertaken using a rheometer (TA, DHR, USA). The rheometer was equipped with a 20 mm stainless steel

upper cone and temperature-controlled Peltier bottom plate (DISCOVERY HR-2, TA, USA), at 37 ^{o}C [62]. A 400 µL aliquot of the solution of SA-CS, Cur-PF127 and PVA was introduced to the Peltier, after which the cone was lowered to a specified gap. Water vapourisation was prevented by placing a low-viscosity oil, after which gelation was initiated using 70 µL of borax (4 wt %) which was injected into the gap. To determine the storage moduli and the gelation kinetics, a dynamic time sweep at 1 Hz at a 1% applied strain for a duration of 2000 s was conducted. The elastic behavior post-gelation of the solutions (now hydrogels) was determined via 0.1-100 rad/s dynamic frequency sweeps at 1 % strain and 0.1 % - 500 % (or to failure) strain sweeps at 1 Hz.

2.8 Drug release profile of the composite hydrogels

The amount of curcumin released from the hydrogels was measured according to the previous report [17]. Briefly, 1 ml of composite hydrogel was immersed in 3 ml of PBS at 37 ^{o}C, and 300 µl of leaching solution was collected at predetermined time intervals. The absorbance of the extract solution was measured by the microplate reader.

2.9 Swelling Test

The freeze-dried hydrogel was introduced to PBS (5 mL) at room temperature and maintained for specified time intervals. At the different time intervals, the hydrogel was recovered and cleaned using filter paper such that additional surface fluid was removed with the swelling ratio (SR) calculated as follows;

$$SR = \frac{W_t - W_0}{W_0} \times 100\%. \qquad (2)$$

Where W_0 and W_t denote the initial mass (g) of the hydrogel after freeze-drying and the final mass (g) of the hydrogel after swelling, respectively.

2.10 Antibacterial activity evaluation

Evaluations of the antibacterial activities of the hydrogels were achieved using gram-positive and gram-negative microbes of *Staphylococcus aureu*s (S. aureus) and *Escherichia coli* (*E. coli*), respectively. The hydrogels were introduced into a Luria Bertani (LB) medium (0.02g/10 mL), after which the diluted bacterial suspension (10 µL) was added. The mixture was then cultured for 12 h at a temperature of 37 ºC. The O.D of the mixture at 600 nm was then measured [63]. For consistency, a blank containing all components described above without the hydrogel was employed as the control group such that the antibacterial ratio (AR) was calculated by the following equation:

$$\text{Antibacterial ratio} = \frac{K_b - K_s}{K_b} \times 100\%. \qquad (3)$$

Where K_b represents the absorption of the blank control group, and *Ks* denotes the absorption of the sample containing the hydrogel.

2.11 Cell migration assay

Evaluation of cell migration and cell viability was achieved using NIH 3T3 cells (CRL-1658^{TM}, ATCC). Dulbecco's modified Eagle's medium (DMEM) containing 10 % fetal bovine serum, 100 µg/ mL streptomycin and 100 U/mL penicillin was used to culture the NIH 3T3 cells under an atmosphere of 5 % CO_2 and a temperature of 37 ºC. Passage 5 cells were then seeded at the 96-well plate, after which 100 µL of hydrogel extract was introduced. The well was then incubated for 24 h at 37 ºC. After 24 h, the liquid fraction was removed, and the residual monolayer was scratched linearly using the sharp tip of the 10 µL pipette. The well was then washed twice using PBS solution

to remove the damaged cells away from the wells, after which 100 μL of fresh medium was added to the linear scratch. The 96-well plate was then incubated for 12 h with changes in the linear scratch observed using an optical microscope and analyzed by Image J software [64].

2.12 Cell viability test

NIH 3T3 cells were cultured with the prepared hydrogels, and the viability of the cells was investigated using CCK-8 after cell seed and culturing for different days was undertaken, and the presence of metabolically active cells was measured via optical density (O.D.) measurements at 450 nm. In the study, the culturing of NIH 3T3 cells in the absence of the hydrogel served as the control group. To culture the NIH 3T3 cells with the hydrogel, soaking of the prepared hydrogels in 75 v/v% of ethanol was undertaken overnight, after which the solvent was replaced with PBS. All hydrogels were then introduced to a 48-well plate (Corning), after which 1 mL of NIH 3TS cells solution (1×10^4 cells/mL), was added to each well. The well was subsequently incubated in a 5 % CO_2 atmosphere at the temperature of 37 ^oC while employing the culture medium as a control. The well samples/solutions were then treated using the CCK-8 kit solution (10 μL) after different days of incubation (i.e. 1 day, 2 days, and 3 days). The treated samples were then incubated at 37 ^oC for 2 h, after which the solutions were transferred to a 96-well plate for the determination of their O.D. values at 450 using a microplate reader.

2.13 Statistical analysis

Three replications for each group were undertaken, and the results were reported

as mean data ± SD. Comparison of the mean values was achieved via one-way analysis of variance (SPSS.22), with pairwise comparison undertaken using the LSD method such that statistical significance was when $p < 0.05$.

3. Results and discussion

3.1 Synthesis and characterization of SA-CS and Cur-PF127

As shown in **Scheme 1**, the preparation of Cur-PF127/SA-CS/PVA composite hydrogels is performed in two stages. To synthesize the sialylated chitosan polymer, sialic acid was grafted to the chitosan backbone via an amidation reaction (**Scheme 1a**), and its successful preparation was demonstrated by ^{1}H NMR analysis. **Figure 1a**, shows significant shifts of the unmodified chitosan at 3.14, 3.6 to 4.04 ppm, which are representative of [H2], [H3] to [H6], protons, respectively [65]. The ^{1}H NMR spectra also show that shifts 1.88, 3.44 and 3.61 ppm were determined for the SA-CS representative of [H6], [H7] to [H8] protons, respectively. The [H9] protons were observed at shifts of 1.67 and 2.04 ppm. Moreover, the successful synthesization of SA-CS was also confirmed by the Fourier-transform infrared spectrometer (FT-IR). As shown in **Figure 1b**, The FT-IR spectrum of CS and SA-CS showed peaks assigned to the saccharide structure at 893.87 cm^{-1} and 1150.36 cm^{-1} [66]. The band, due to angular deformation of N-H (1617.97 cm-1), was quite reduced for SA-CS, which was caused by grafting sialic acid to the primary amine. Moreover, a new absorption peak in the FT-IR spectrum appeared at 2912.83 cm^{-1}, corresponding to the C-H stretching of the methyl group of sialic acid. The results demonstrate the successful grafting of the SA

to the backbone of CS. As stated earlier above, curcumin possesses several poor characteristics (e.g poor solubility in **Figure 1c**), while the present study employing an amphiphilic triblock copolymer PF127 for curcumin encapsulation as a pathway for preparing curcumin-PF127 micelles (Cur-PF127) formation (**Scheme 1b**). The Cur-PF127 micelle solution was shown to have good solubility up to 3 mg/mL with the resulting TEM images of the resulting Cur-PF127 micelles presented in **Figures 1d** and **1e**. **Figures 1e** and **f** showed that Cur-PF127 micelles manifested sphere-like shapes with a diameter of ~33.5 ± 4.2 nm.

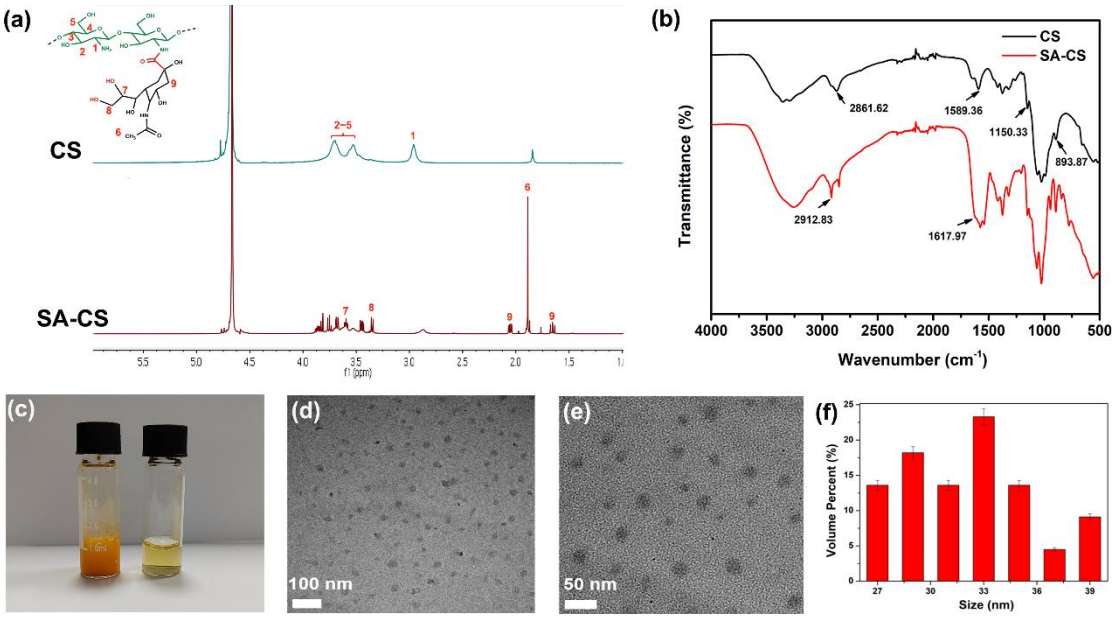

Figure. 1 Illustration of SA-CS and Cur-PF127 micelles. (a) ^{1}H NMR spectra of CS and SA-CS. (b) FT-IR spectra of CS and SA-CS. (c) Images of free curcumin (on the left) and Cur-PF127 micelles (on the right) in water. (d, e) TEM images using different magnifications of Cur-PF127 micelles, and (f) size distribution of Cur-PF127 micelles calculated from TEM images.

3.2 Physicochemical properties of hydrogels

The SA-CA/Cur-PF127/PVA composite hydrogels were synthesized by mixing

SA-CS, PVA, Cur-PF127 and borax at physiological conditions (**Scheme 1c**), in which borax could form dynamic boron-diol bonds with PVA and SA-CS. As depicted in **Figure 2a**, the hydrogel was formed by adding borax solution into PVA/SA-CS/Cur-PF127 solution, and the hydrogel formation was confirmed via the tube inversion method [50, 62]. SEM images were used to observe the morphology of the lyophilized composite hydrogels (**Figure 2b**). The highly porous structure promotes cell migration. It was also observed that the introduction of Cur-PF127 micelles led to a decrease in the pore size and porosity of the composite hydrogel, although the structural connections improved. The lyophilised hydrogels' three-dimensional (3D) structure with interconnected pore structures facilitates water absorption, oxygen and nutrient exchange, and cell migration and growth, providing conditions for the rapid healing of different wound tissues.

The prepared composite hydrogels showed a reversible building of dynamic covalent bonds responsible for their self-healing. For instance, the hydrogel Gel 1 was cut and divided, and the divided two parts, when contacted, maintained integrity in some time (**Figure 2c**). **Figure 2d** shows that all hydrogels attained an equilibrium swelling state at one hour, with this equilibrium swelling rate maintained over time, thus highlighting the favorable dimensional stability of the hydrogels. Hydrogels Gel 1, Gel 2, and Gel 3 showed equilibrium swelling rates of 370 ± 5 %, 550 ±10 %, and 600 ± 9 %, respectively. It is worth noting that Gel 4 collapsed during the swelling test due to its frail structure, and the swelling ratio data are not shown in **Figure 2d**.

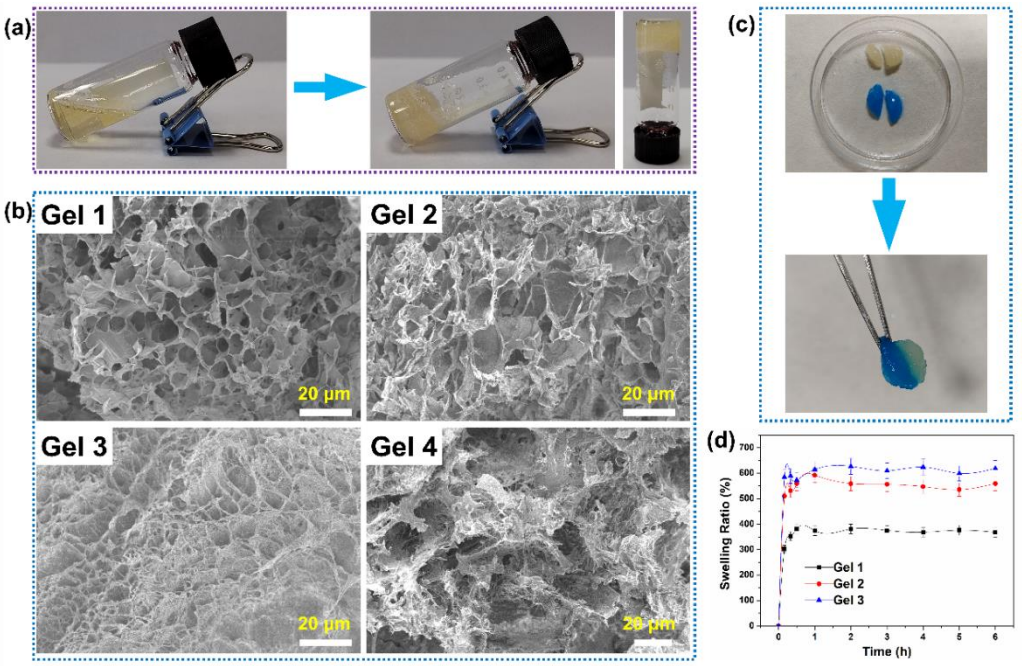

Figure 2. (a) The prepared hydrogel formation was shown by the vial inversion approach (sample Gel 1 was displayed). (b) Photos highlight the self-healing process of hydrogels (sample Gel 1). (c) SEM images of the hydrogels (Gel 1, Gel 2, Gel 3, and Gel 4). (d) Swelling behaviors of the hydrogels (Gel 1, Gel 2, and Gel 3), it was noted that the swelling data of Gel 4 was shown due to the collapse during the swelling test.

The viscoelastic properties of the prepared composite hydrogels containing Cur-PF127 micelles were tested using rheological measurement (**Figure 3**). **Figures 3a** and **3b**, showed the G' and G" values of the composite hydrogels during the gelation when 1 % strain and 1 Hz frequency were imposed for 2000 s. It showed a marginal reduction in the G' and G" as the amount of Cur-PF127 in the composite hydrogels was increased. The frequency sweep results showed that slight increments in G' and G'' were observed as the frequency increased, with G' > G" maintained in the range of 1-10 rad/s (**Figures 3c** and **3d**). This indicated that the hydrogels were predominantly elastic. G' kept relatively stable and was greater than G" in an extensive range of strain, representing

the favorable elastic property. During the hydrogel formation process, as the time or shear frequency increased, the peak of G' decreased alongside the increase in Cur-PF127 concentration, which was also visible in the amplitude sweep test (**Figures 3e** and **3f**).

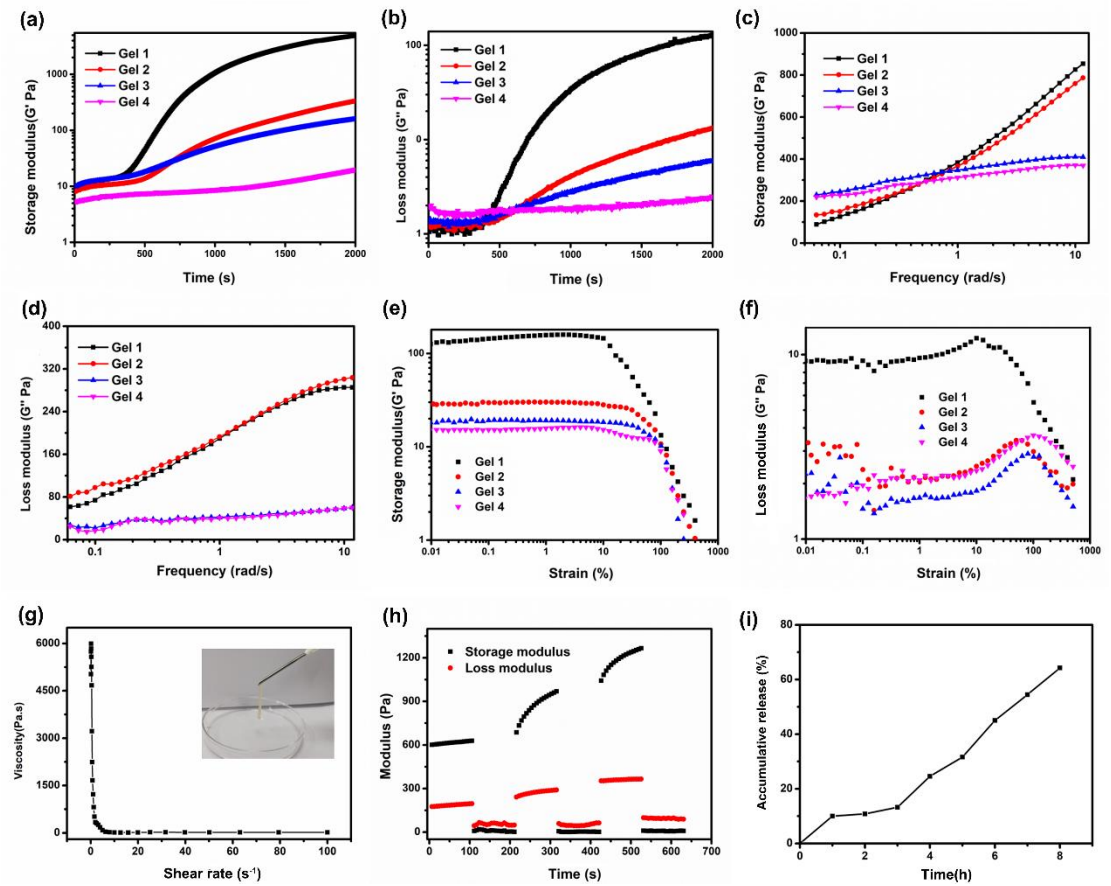

Figure 3. Rheology analysis of the hydrogels. (a, b) Storage modulus (G') and loss modulus (G") of hydrogels on time sweep for 2000 s at the stain of 1 % and the frequency with 1 Hz. (c, d) G' and G" of hydrogels on frequency sweep from 1 to 10 rad/s at the strain of 1 %. (e, f) G' and G" of hydrogels on strain sweep from 0.1 % to 1000 % at the frequency of 1 Hz. (g) The viscosity change of Gel 1 in terms of shear rate, and inserted photograph displays hydrogel during injection. (h) G′ and G" of Gel 1 on continuous time sweep with alternate strain for three cycles (low strain at 1 % for 100 s and high strain at 300 % for 100 s). (i) Release profile of Cur-PF127 micelles in the Gel

3.

Figure 2g shows that an increase in the shear rate leads to a decrease in the viscosity of the hydrogel, which is indicative of the shear thinning characteristic and thus highlights the injectability of the hydrogels. In **Figure 2h**, The continuous step strain method was used to assess the rheological recovery behavior of the hydrogel. Taking Gel 1 for example, the G' value was more extensive than G" when a low strain of 1% strain was imposed, representing the stable of the hydrogel. However, when a high strain of 300% was imposed, the values of G' was greater than G", meaning the collapse of the structure of hydrogel. Interestingly, the hydrogels returned to the initial state of G' > G" when the strain is returned to 1%. These observations indicated that the hydrogel had the self-healing property and shear thining behavior owing to the dynamic and reversible borate-diol bonds between borate and SA-CS. To achieve an effective therapeutic effect, a prolonged release of curcumin is appreciated at the wound. In **Figure 3i**, Gel 3 showed stable and sustained release behaviour without significant burst release, and the release rate was about 60 % in 9 h. In the same test, the amount of Cur-PF127 from Gel 2 was too low to detect, and Gel 4 structure broke down. Therefore, Our result also proved that a higher addition of Cur-PF127 micelles may impair the rheological properties and 3D network structure.

3.3 Antioxidant and antibacterial properties

Figure 4a shows that, as expected, a positive correlation exists between the increasing concentrations of curcumin and antioxidant ability. Similarly, in all cases, a positive correlation existed between the increasing concentrations of curcumin and the

killing ratio was observed. Thus, all prepared hydrogels demonstrated antibacterial properties with the increase in the amount of Cur-PFA127. The antibacterial ratio of Gel 2 and Gel 3 was shown to be more proficient in killing *S. aureus* than *E.coli* , with a reverse trend observed in Gel 1.

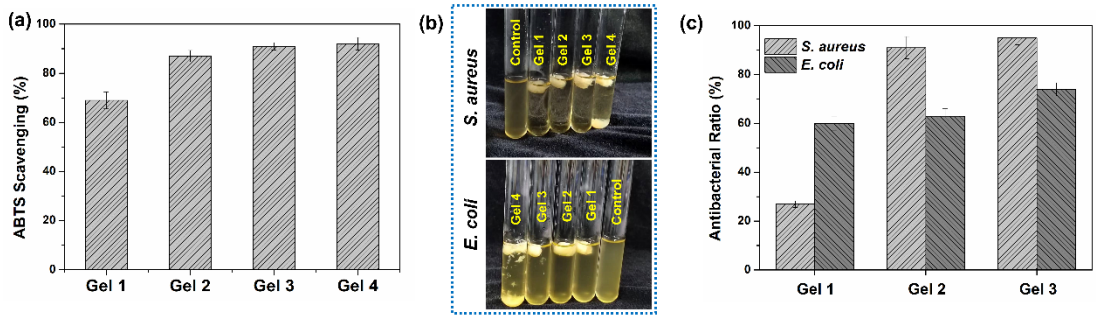

Figure 4. (a) ABTS scavenging of the hydrogels. The antibacterial behavior of the composite hydrogels (sterilized 0.9 % saline solution was taken as the control group) after 12 h. (b) Photographs of *S. aureus* and *E. coli* with hydrogels grown in the actual culture tube for 12 h. (c) The antibacterial activity of the hydrogels against *S. aureus* and *E. coli* after 12 h, the data of Gel 4 was not shown because that Gel 4 collapsed during the test.

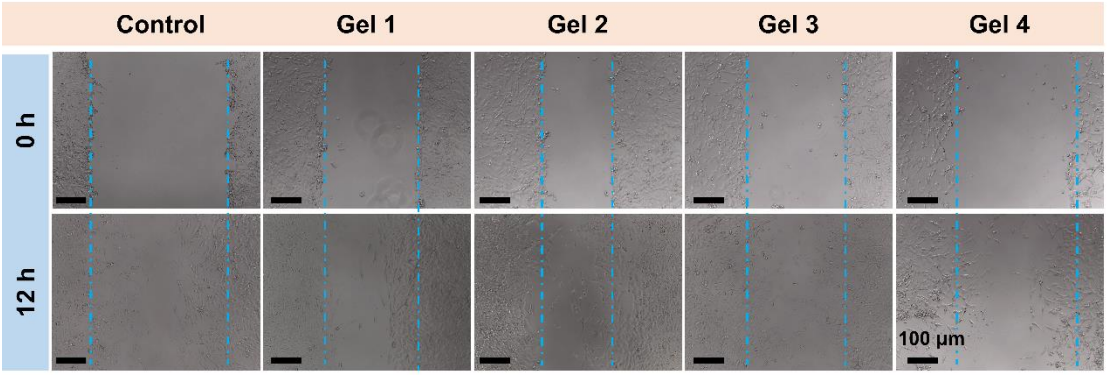

Figure 5. NIH 3T3 cells scratch test with, the blue dotted lines indicating the scratch gap width. Scar bar: 100 μm.

3.4 Scratch assay of NIH 3TS

Figure 5 shows that, relative to the blank group, Gel 1, Gel 2, and Gel 3 showed

improved NIH 3T3 cell migration, leading to faster cell-free gap closure, thus highlighting the potential for the hydrogels to promote wound healing. Interestingly, the effect of Gel 4 with a higher amount of Cur-PF127 on cell migration was not as obvious as that of Gel 2 and Gel 3.

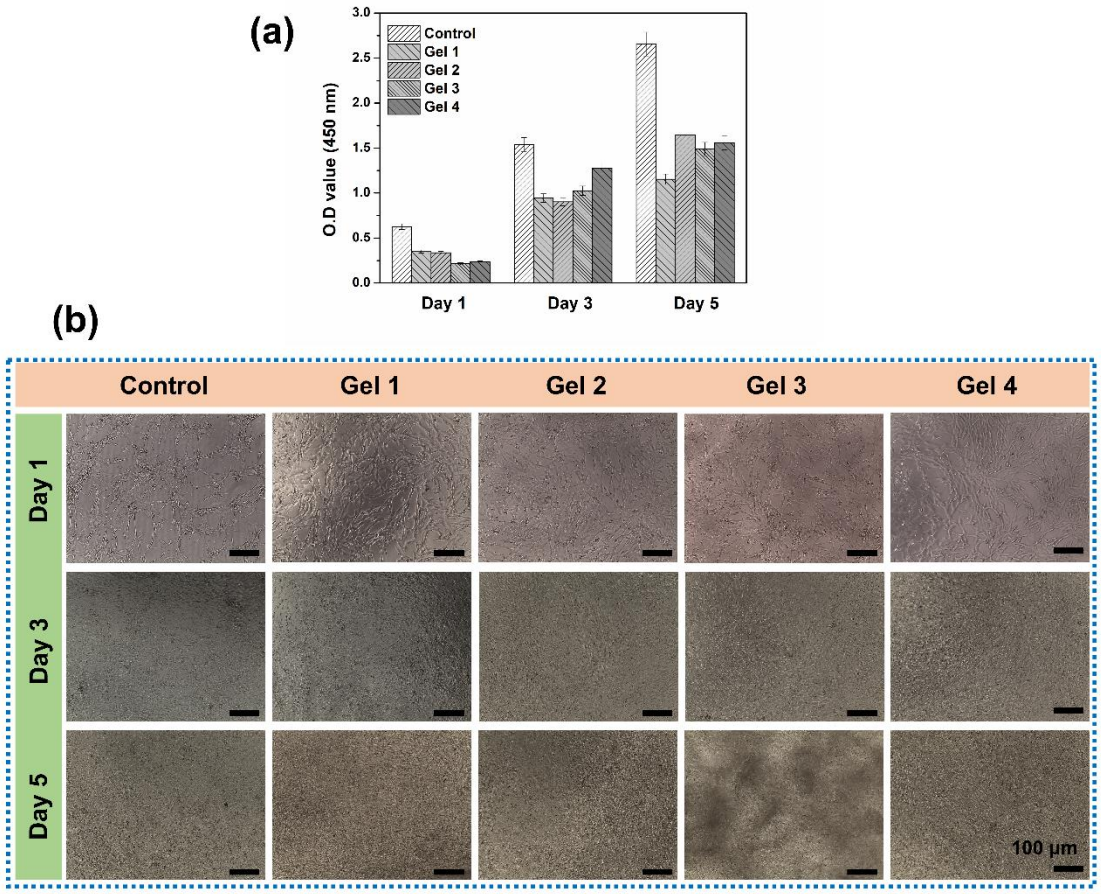

Figure 6. (a) Cytocompatibility of the hydrogels after being cultured with NIH 3T3 cells for different days through CCK8 method. (b) Representative pictures of NIH 3T3 cells cultured with the composite hydrogels on days 1, 3, and 5.

3.5 Cytotoxicity of the hydrogels

NIH 3T3 cells were grown on the surface of the hydrogels, and the impact of the hydrogels on cell proliferation was subsequently assessed via CCK-8 assays (**Figure 6**). The results showed that overall cell proliferation was promoted on the surface of

each of the prepared hydrogels. It can therefore be deduced that the overall cell proliferation trend in the prepared composite hydrogels was favourable, indicating that they were not cytotoxic and had good biocompatibility.

4. Conclusions

A polysaccharide-based composite hydrogel delivery system based on PVA, SA-CS, and curcumin-loaded Pluronic F127 micelles was prepared as a possible pathway for enhanced skin wound healing. Based on the dynamic boronic ester bond formation between PVA, SA-CS and borax, the hydrogels showed stable rheological properties, tunable mechanical properties, biocompatibility, free radical scavenging capacity, and favorable antibacterial property at physiological conditions. These properties highlight the potential for the future application of hydrogel in wound healing.

Declaration of competing interest

The authors declare that they have no known competing financial interests or personal relationships that could have appeared to influence the work reported in this paper.

Data availability

Data will be made available on request.

Acknowledgments

The authors acknowledge support from the Nanhu Scholars Program for Young

Scholars of XYNU. This research was supported by the Key Scientific Research Projects of Higher Education Institutions in Henan Province (24A430034). The authors acknowledge the help from Prof Lingling Wang, Prof. Qiuju Zhou, Miss Zihe Jin, Dr. Zongwen Zhang, and Dr. Dongli Xu, in the Analysis & Testing Center of XYNU.

References

[1] M. Abbas, T. Hussain, M. Arshad, A.R. Ansari, A. Irshad, J. Nisar, F. Hussain, N. Masood, A. Nazir, M. Iqbal, Wound healing potential of curcumin cross-linked chitosan/polyvinyl alcohol, International Journal of Biological Macromolecules, 140 (2019) 871-876.

[2] D.M. Brogan, E. Mossialos, A critical analysis of the review on antimicrobial resistance report and the infectious disease financing facility, Globalization and Health, 12 (2016).

[3] M. Luo, M. Wang, W. Niu, M. Chen, W. Cheng, L. Zhang, C. Xie, Y. Wang, Y. Guo, T. Leng, X. Zhang, C. Lin, B. Lei, Injectable self-healing anti-inflammatory europium oxide-based dressing with high angiogenesis for improving wound healing and skin regeneration, Chemical Engineering Journal, 412 (2021) 128471.

[4] M. Shahriari-Khalaji, G. Li, L. Liu, M. Sattar, L. Chen, C. Zhong, F.F. Hong, A poly-l-lysine-bonded TEMPO-oxidized bacterial nanocellulose-based antibacterial dressing for infected wound treatment, Carbohydrate Polymers, 287 (2022) 119266.

[5] M. Sheikholeslam, M.E.E. Wright, M.G. Jeschke, S. Amini-Nik, Biomaterials for Skin Substitutes, Advanced Healthcare Materials, 7 (2018) 1700897.

[6] K. Wu, M. Fu, Y. Zhao, E. Gerhard, Y. Li, J. Yang, J. Guo, Anti-oxidant anti-inflammatory and antibacterial tannin-crosslinked citrate-based mussel-inspired bioadhesives facilitate scarless wound healing, Bioactive Materials, 20 (2023) 93-110.

[7] Y. Xie, K. Qiao, L. Yue, T. Tang, Y. Zheng, S. Zhu, H. Yang, Z. Fang, A self-crosslinking, double-functional group modified bacterial cellulose gel used for antibacterial and healing of infected wound, Bioactive Materials, 17 (2022) 248-260.

[8] R. Xu, G. Luo, H. Xia, W. He, J. Zhao, B. Liu, J. Tan, J. Zhou, D. Liu, Y. Wang, Z. Yao, R. Zhan, S. Yang, J. Wu, Novel bilayer wound dressing composed of silicone rubber with particular micropores enhanced wound re-epithelialization and contraction, Biomaterials, 40 (2015) 1-11.

[9] L. Zhou, H. Zheng, Z. Liu, S. Wang, Z. Liu, F. Chen, H. Zhang, J. Kong, F. Zhou, Q. Zhang, Conductive Antibacterial Hemostatic Multifunctional Scaffolds Based on Ti3C2Tx MXene Nanosheets for Promoting Multidrug-Resistant Bacteria-Infected Wound Healing, ACS Nano, 15 (2021) 2468-2480.

[10] S. Liu, Y. Zhao, M. Li, L. Nie, Q. Wei, O.V. Okoro, H. Jafari, S. Wang, J. Deng, J. Chen, Bioactive wound dressing based on decellularized tendon and GelMA with incorporation of PDA-loaded asiaticoside nanoparticles for scarless wound healing, Chemical Engineering Journal, 466 (2023) 143016.

[11] L. Nie, Q. Wei, J. Li, Y. Deng, X. He, X. Gao, X. Ma, S. Liu, Y. Sun, G. Jiang, Fabrication and desired properties of conductive hydrogel dressings for wound healing, Rsc Adv, 13 (2023) 8502-8522.

[12] B.-D. Zheng, J. Ye, Y.-C. Yang, Y.-Y. Huang, M.-T. Xiao, Self-healing polysaccharide-based injectable hydrogels with antibacterial activity for wound healing, Carbohydrate Polymers, 275 (2022) 118770.

[13] C. Gong, Q. Wu, Y. Wang, D. Zhang, F. Luo, X. Zhao, Y. Wei, Z. Qian, A biodegradable hydrogel system containing curcumin encapsulated in micelles for cutaneous wound healing, Biomaterials, 34 (2013) 6377-6387.

[14] O. Castaño, S. Pérez-Amodio, C. Navarro-Requena, M.Á. Mateos-Timoneda, E. Engel, Instructive microenvironments in skin wound healing: Biomaterials as signal releasing platforms, Advanced Drug Delivery Reviews, 129 (2018) 95-117.

[15] J.C. Brazil, M. Quiros, A. Nusrat, C.A. Parkos, Innate immune cell–epithelial crosstalk during wound repair, Journal of Clinical Investigation, 129 (2019) 2983-2993.

[16] X. Zhao, Y. Yang, J. Yu, R. Ding, D. Pei, Y. Zhang, G. He, Y. Cheng, A. Li, Injectable hydrogels with high drug loading through B–N coordination and ROS-triggered drug release for efficient treatment of chronic periodontitis in diabetic rats, Biomaterials, 282 (2022) 121387.

[17] X. Zhang, J. Feng, W. Feng, B. Xu, K. Zhang, G. Ma, Y. Li, M. Yang, F.-J. Xu, Glycosaminoglycan-Based Hydrogel Delivery System Regulates the Wound Microenvironment to Rescue Chronic Wound Healing, ACS Applied Materials & Interfaces, 14 (2022) 31737-31750.

[18] Y. Yang, K. Shi, K. Yu, F. Xing, H. Lai, Y. Zhou, P. Xiao, Degradable Hydrogel Adhesives with Enhanced Tissue Adhesion, Superior Self‐Healing,

Cytocompatibility, and Antibacterial Property, Advanced Healthcare Materials, 11 (2021) 2101504.

[19] Y. Wang, J. Guo, B. Li, D. Li, Z. Meng, S.-K. Sun, Biocompatible therapeutic albumin/genipin bioglue for postoperative wound adhesion and residual tumor ablation, Biomaterials, 279 (2021) 121179.

[20] Z. Tu, M. Chen, M. Wang, Z. Shao, X. Jiang, K. Wang, Z. Yao, S. Yang, X. Zhang, W. Gao, C. Lin, B. Lei, C. Mao, Engineering Bioactive M2 Macrophage‐Polarized Anti‐Inflammatory, Antioxidant, and Antibacterial Scaffolds for Rapid Angiogenesis and Diabetic Wound Repair, Advanced Functional Materials, 31 (2021).

[21] N. Tang, R. Zhang, Y. Zheng, J. Wang, M. Khatib, X. Jiang, C. Zhou, R. Omar, W. Saliba, W. Wu, M. Yuan, D. Cui, H. Haick, Highly Efficient Self‐Healing Multifunctional Dressing with Antibacterial Activity for Sutureless Wound Closure and Infected Wound Monitoring, Advanced Materials, 34 (2021) 2106842.

[22] Y. Qian, Y. Zheng, J. Jin, X. Wu, K. Xu, M. Dai, Q. Niu, H. Zheng, X. He, J. Shen, Immunoregulation in Diabetic Wound Repair with a Photoenhanced Glycyrrhizic Acid Hydrogel Scaffold, Advanced Materials, 34 (2022) 2200521.

[23] L.J. Pruett, C.H. Jenkins, N.S. Singh, K.J. Catallo, D.R. Griffin, Heparin Microislands in Microporous Annealed Particle Scaffolds for Accelerated Diabetic Wound Healing, Advanced Functional Materials, 31 (2021) 2104337.

[24] J. Liu, M. Qu, C. Wang, Y. Xue, H. Huang, Q. Chen, W. Sun, X. Zhou, G. Xu, X. Jiang, A Dual‐Cross‐Linked Hydrogel Patch for Promoting Diabetic Wound Healing, Small, 18 (2022) 2106172.

[25] G. Liu, L. Wang, Y. He, L. Wang, Z. Deng, J. Liu, D. Peng, T. Ding, L. Lu, Y. Ding, J. Zhang, P. Liu, K. Cai, Polydopamine Nanosheets Doped Injectable Hydrogel with Nitric Oxide Release and Photothermal Effects for Bacterial Ablation and Wound Healing, Advanced Healthcare Materials, 10 (2021) 2101476.

[26] X. Feng, X. Zhang, S. Li, Y. Zheng, X. Shi, F. Li, S. Guo, J. Yang, Preparation of aminated fish scale collagen and oxidized sodium alginate hybrid hydrogel for enhanced full-thickness wound healing, International Journal of Biological Macromolecules, 164 (2020) 626-637.

[27] B. Hu, C. Berkey, T. Feliciano, X. Chen, Z. Li, C. Chen, S. Amini, M.H. Nai, Q.L. Lei, R. Ni, J. Wang, W.R. Leow, S. Pan, Y.Q. Li, P. Cai, A. Miserez, S. Li, C.T. Lim, Y.L. Wu, T.W. Odom, R.H. Dauskardt, X. Chen, Thermal‐Disrupting Interface Mitigates Intercellular Cohesion Loss for Accurate Topical Antibacterial Therapy, Advanced Materials, 32 (2020) 1907030.

[28] A.-T. Iacob, M. Drăgan, O.-M. Ionescu, L. Profire, A. Ficai, E. Andronescu, L.G. Confederat, D. Lupaşcu, An Overview of Biopolymeric Electrospun Nanofibers Based on Polysaccharides for Wound Healing Management, Pharmaceutics, 12 (2020) 983.

[29] M. Li, J. Chen, M. Shi, H. Zhang, P.X. Ma, B. Guo, Electroactive anti-oxidant polyurethane elastomers with shape memory property as non-adherent wound dressing to enhance wound healing, Chemical Engineering Journal, 375 (2019) 121999.

[30] A. Moeini, P. Pedram, P. Makvandi, M. Malinconico, G. Gomez d'Ayala, Wound healing and antimicrobial effect of active secondary metabolites in chitosan-based wound dressings: A review, Carbohydrate Polymers, 233 (2020) 115839.

[31] C. Xuan, L. Hao, X. Liu, Y. Zhu, H. Yang, Y. Ren, L. Wang, T. Fujie, H. Wu, Y. Chen, X. Shi, C. Mao, Wet-adhesive, haemostatic and antimicrobial bilayered composite nanosheets for sealing and healing soft-tissue bleeding wounds, Biomaterials, 252 (2020) 120018.

[32] I. Eugenis, D. Wu, T.A. Rando, Cells, scaffolds, and bioactive factors: Engineering strategies for improving regeneration following volumetric muscle loss, Biomaterials, 278 (2021) 121173.

[33] M. Zhu, W. Zhong, W. Cao, Q. Zhang, G. Wu, Chondroinductive/chondroconductive peptides and their-functionalized biomaterials for cartilage tissue engineering, Bioactive materials, 9 (2022) 221-238.

[34] L. Siebert, E. Luna‐Cerón, L.E. García‐Rivera, J. Oh, J. Jang, D.A. Rosas‐Gómez, M.D. Pérez‐Gómez, G. Maschkowitz, H. Fickenscher, D. Oceguera‐Cuevas, C.G. Holguín‐León, B. Byambaa, M.A. Hussain, E. Enciso‐Martínez, M. Cho, Y. Lee, N. Sobahi, A. Hasan, D.P. Orgill, Y.K. Mishra, R. Adelung, E. Lee, S.R. Shin, Light‐Controlled Growth Factors Release on Tetrapodal ZnO‐Incorporated 3D‐Printed Hydrogels for Developing Smart Wound Scaffold, Advanced Functional Materials, 31 (2021) 2007555.

[35] H. Zhang, X. Sun, J. Wang, Y. Zhang, M. Dong, T. Bu, L. Li, Y. Liu, L. Wang, Multifunctional Injectable Hydrogel Dressings for Effectively Accelerating Wound Healing: Enhancing Biomineralization Strategy, Advanced Functional Materials, 31 (2021) 2100093.

[36] Q. Xuan, F. Jiang, H. Dong, W. Zhang, F. Zhang, T. Ma, J. Zhuang, J. Yu, Y. Wang, H. Shen, C. Chen, P. Wang, Bioinspired Intrinsic Versatile Hydrogel Fabricated by Amyloidal Toxin Simulant‐Based Nanofibrous Assemblies for Accelerated Diabetic Wound Healing, Advanced Functional Materials, 31 (2021) 2106705.

[37] P. Ghaffari-Bohlouli, H. Alimoradi, D.F.S. Petri, S. Moghassemi, C.A. Amorim, L. Nie, A. Shavandi, Alleviating hypoxia through self-generating oxygen and hydrogen peroxide fluorinated chitosan: Insights from a kinetic study, Chemical Engineering Journal, (2023) 145072.

[38] P. Ghaffari-Bohlouli, J. Simińska-Stanny, H. Jafari, M. Mirzaei, L. Nie, C. Delporte, A. Shavandi, Printable hyaluronic acid hydrogel functionalized with yeast-derived peptide for skin wound healing, International journal of biological macromolecules, 232 (2023) 123348.

[39] J. Radhakrishnan, A. Subramanian, U.M. Krishnan, S. Sethuraman, Injectable and 3D Bioprinted Polysaccharide Hydrogels: From Cartilage to Osteochondral Tissue Engineering, Biomacromolecules, 18 (2016) 1-26.

[40] A. Fabiano, D. Beconcini, C. Migone, A.M. Piras, Y. Zambito, Quaternary Ammonium Chitosans: The Importance of the Positive Fixed Charge of the Drug Delivery Systems, International Journal of Molecular Sciences, 21 (2020) 6617.

[41] S. Rashki, K. Asgarpour, H. Tarrahimofrad, M. Hashemipour, M.S. Ebrahimi, H. Fathizadeh, A. Khorshidi, H. Khan, Z. Marzhoseyni, M. Salavati-Niasari, H. Mirzaei, Chitosan-based nanoparticles against bacterial infections, Carbohydrate Polymers, 251 (2021) 117108.

[42] R. Parhi, Drug delivery applications of chitin and chitosan: a review, Environmental Chemistry Letters, 18 (2020) 577-594.

[43] M.F.P. Graça, S.P. Miguel, C.S.D. Cabral, I.J. Correia, Hyaluronic acid—Based wound dressings: A review, Carbohydrate Polymers, 241 (2020) 116364.

[44] A. Gilarska, J. Lewandowska-Łańcucka, K. Guzdek-Zając, A. Karewicz, W. Horak, R. Lach, K. Wójcik, M. Nowakowska, Bioactive yet antimicrobial structurally stable collagen/chitosan/lysine functionalized hyaluronic acid – based injectable hydrogels for potential bone tissue engineering applications, International Journal of Biological Macromolecules, 155 (2020) 938-950.

[45] S. Yan, T. Wang, L. Feng, J. Zhu, K. Zhang, X. Chen, L. Cui, J. Yin, Injectable In Situ Self-Cross-Linking Hydrogels Based on Poly(l-glutamic acid) and Alginate for Cartilage Tissue Engineering, Biomacromolecules, 15 (2014) 4495-4508.

[46] Y. Fu, J. Zhang, Y. Wang, J. Li, J. Bao, X. Xu, C. Zhang, Y. Li, H. Wu, Z. Gu, Reduced polydopamine nanoparticles incorporated oxidized dextran/chitosan hybrid hydrogels with enhanced antioxidative and antibacterial properties for accelerated wound healing, Carbohydrate Polymers, 257 (2021) 117598.

[47] G. Liu, Y. Zhou, Z. Xu, Z. Bao, L. Zheng, J. Wu, Janus hydrogel with dual antibacterial and angiogenesis functions for enhanced diabetic wound healing. Chinese Chemical Letters, 34 (2023) 107705.

[48] Y. Fang, G. Li, C. Huang, K. Huang, Y. Zhao, T. Nie and J. Wu, Tomato based gelatin methacryloyl hydrogel as an effective natural and low-cost scaffold for

accelerative wound healing. International Journal of Biological Macromolecules, 229 (2023) 123-135.

[49] P. Xin, S. Han, J. Huang, C. Zhou, J. Zhang, X. You, J. Wu, Natural okra-based hydrogel for chronic diabetic wound healing. Chinese Chemical Letters, 34 (2023) 108125.

[50] R. Jayakumar, K.P. Chennazhi, S. Srinivasan, S.V. Nair, T. Furuike, H. Tamura, Chitin Scaffolds in Tissue Engineering, International Journal of Molecular Sciences, 12 (2011) 1876-1887.

[51] S. Islam, M.A.R. Bhuiyan, M.N. Islam, Chitin and Chitosan: Structure, Properties and Applications in Biomedical Engineering, Journal of Polymers and the Environment, 25 (2016) 854-866.

[52] H. Nosrati, M. Khodaei, Z. Alizadeh, M. Banitalebi-Dehkordi, Cationic, anionic and neutral polysaccharides for skin tissue engineering and wound healing applications, International Journal of Biological Macromolecules, 192 (2021) 298-322.

[53] Q. Wu, L. Wang, P. Ding, Y. Deng, O.V. Okoro, A. Shavandi, L. Nie, Mercaptolated chitosan/methacrylate gelatin composite hydrogel for potential wound healing applications, Composites Communications, 35 (2022) 101344.

[54] H. Jafari, P. Ghaffari-Bohlouli, D. Podstawczyk, L. Nie, A. Shavandi, Tannic acid post-treatment of enzymatically crosslinked chitosan-alginate hydrogels for biomedical applications, Carbohydrate polymers, 295 (2022) 119844.

[55] C. Mohanty, S.K. Sahoo, Curcumin and its topical formulations for wound healing applications, Drug Discovery Today, 22 (2017) 1582-1592.

[56] D. Akbik, M. Ghadiri, W. Chrzanowski, R. Rohanizadeh, Curcumin as a wound healing agent, Life Sciences, 116 (2014) 1-7.

[57] V. Kant, A. Gopal, N.N. Pathak, P. Kumar, S.K. Tandan, D. Kumar, Antioxidant and anti-inflammatory potential of curcumin accelerated the cutaneous wound healing in streptozotocin-induced diabetic rats, International Immunopharmacology, 20 (2014) 322-330.

[58] Z. Hussain, H.E. Thu, S.-F. Ng, S. Khan, H. Katas, Nanoencapsulation, an efficient and promising approach to maximize wound healing efficacy of curcumin: A review of new trends and state-of-the-art, Colloids and Surfaces B: Biointerfaces, 150 (2017) 223-241.

[59] J. Qu, X. Zhao, Y. Liang, T. Zhang, P.X. Ma, B. Guo, Antibacterial adhesive injectable hydrogels with rapid self-healing, extensibility and compressibility as wound dressing for joints skin wound healing, Biomaterials, 183 (2018) 185-199.

[60] S. Shen, D. Fan, Y. Yuan, X. Ma, J. Zhao, J. Yang, An ultrasmall infinite coordination polymer nanomedicine-composited biomimetic hydrogel for programmed dressing-chemo-low level laser combination therapy of burn wounds, Chemical Engineering Journal, 426 (2021) 130610.

[61] O. Naksuriya, S. Okonogi, R.M. Schiffelers, W.E. Hennink, Curcumin nanoformulations: A review of pharmaceutical properties and preclinical studies and clinical data related to cancer treatment, Biomaterials, 35 (2014) 3365-3383.

[62] J. Zhou, Z. Wang, C. Yang, H. Zhang, M.S. Fareed, Y. He, J. Su, P. Wang, Z. Shen, W. Yan, K. Wang, A carrier-free, dual-functional hydrogel constructed of antimicrobial

peptide Jelleine-1 and 8Br-cAMP for MRSA infected diabetic wound healing, Acta Biomaterialia, 151 (2022) 223-234.

[63] L. Nie, Q. Wei, M. Sun, P. Ding, L. Wang, Y. Sun, X. Ding, O.V. Okoro, G. Jiang, A. Shavandi, Injectable, self-healing, transparent, and antibacterial hydrogels based on chitosan and dextran for wound dressings, Int J Biol Macromol, 233 (2023) 123494.

[64] M. Sun, S. Peng, C. Zhao, J. Huang, J. Xia, D. Ye, X. Dou, W. Hou, C. Feng, Herb‐Functionalized Chronic Wound Dressings for Enhancing Biological Functions: Multiple Flavonoids Coordination Driven Strategy, Advanced Functional Materials, 32 (2022) 2204291.

[65] G. Qing, X. Li, P. Xiong, C. Chen, M. Zhan, X. Liang, T Sun, Dipeptide-based carbohydrate receptors and polymers for glycopeptide enrichment and glycan discrimination. ACS Applied Materials & Interfaces, 8 (2016) 22084-22092.

[66] P. Mondal, K. Chatterjee, Injectable and self-healing double network polysaccharide hydrogel as a minimally-invasive delivery platform[J]. Carbohydrate Polymers, 2022, 291: 119585.